MKID Large Format Array Testbed

Ferrari, Lorenza; Yates, Stephen J.C.; Eggens, Martin; Baryshev, Andrey M.; Baselmans, Jochem J.A.

DOI
10.1109/TTHZ.2018.2871365

Publication date
2018

Document Version
Final published version

Published in
IEEE Transactions on Terahertz Science and Technology

MKID Large Format Array Testbed

Lorenza Ferrari, Stephen J. C. Yates, Martin Eggens, Andrey M. Baryshev, and Jochem J. A. Baselmans

***Abstract*—The development of astrophysics kilo-pixel imaging systems requires a dedicated cryogenics and optics setup to measure the performance of the detector arrays in terms of sensitivity, crosstalk, dynamic range, and spatial response. We have developed such testbed for the characterization of large format arrays of microwave kinetic inductance detectors (MKIDs), capable of measuring detector chips of 6 cm × 6 cm, operating in the 350 and 850 GHz band. The testbed is a wide field camera that produces an aberration free image of the chip outside of the cryostat. The cryostat is based upon a commercial pulse-tube cooled 3 K system with an He3-He3-He4 sorption cooler that reaches a base temperature below 250 mK. We will describe the thermomechanical solutions implemented in our system to minimize the thermal loading on the cold stage, needed to reach the low base temperature. We will also give the optical design including straylight control.**

***Index Terms*—Cryostat, detector, test bed, submm.**

I. Introduction

FUTURE and present submm- and mm-wave astronomical instruments benefit enormously from the developments in detector technology. The increased availability of large format arrays of ultrasensitive detectors fulfills the need for maximizing science output through high on-sky scanning speed. In the last decade, microwave kinetic inductance detectors (MKIDs) [1] are emerging as an excellent choice due to their intrinsic multiplexing capability, which makes the readout of kilopixel arrays relatively simple and cheap compared to other technologies [2], [3]. Instruments like MUSIC [4] or NIKA [5] and NIKA 2 [6] are showing the potential of this approach in the astronomical field. At SRON, we are developing lens-antenna coupled KIDs currently optimized for radiation coupling at 350 GHz and at 850 GHz for operation in the AMKID camera [7] for the APEX telescope [8]. A detailed description of the single pixel design can be found in [9] and [10]. The targeted frequencies are at the center of two atmospheric windows accessible from high altitude ground-based sites, and particularly interesting for the study of young systems either in early stage of in-star formation or high redshift galaxies. In general, our design and developments are targeting telescopes such as APEX or future high altitude telescopes such as CCAT [11] or At-LAST [12]. All are located at Llano Chajnantor, Chile, known to have good and very dry weather conditions that are absolutely necessary for observations in high frequency telluric windows. Before deployment to the telescope, the arrays need optical and electrical characterization. The full performance verification requires tests in a wide field camera, which recreates the thermal and optical interfaces of the final AMKID camera. Only in this way, we can link the measurements obtained in the laboratory to the expected instrument performance. With this goal in mind, we have developed the testbed and in this paper we will describe the thermal, optical, and mechanical solutions implemented. We start the paper by describing the cryostat conceptual design based on the specification derived from the telescope instrument and the detector design. In the sections following this, we will describe in detail each cryostat subcomponent.

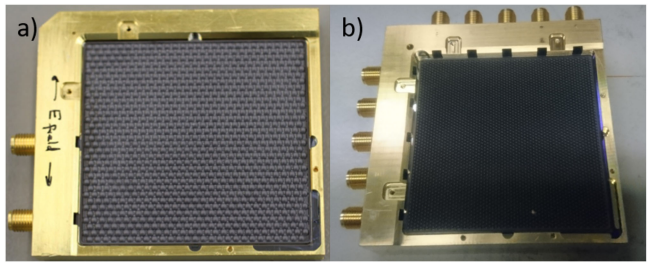

Fig. 1. (a) Assembled LF detector holder with lens array and SMA connectors for contacting the readout circuitry. (b) Assembled detector holder for the HF band. The holders are 58 mm × 58 mm.

II. Design Concept

The testbed is designed to measure KID arrays of 6 × 6 cm^2, the size of one of the four subarrays forming the AMKID focal plane (see Fig. 1), at two frequency bands of 350 and 850 GHz, respectively. The system operates in a single band; switching between frequency bands is realized by the substitution of few quasioptical filters that define the selected radiation band. The cryostat is equipped with five readout chains, which translates into the capability of reading out up to 5000 detectors simultaneously, assuming a state-of-the-art multiplexing ratio of 1000 pixels per readout chain [13]. The optical coupling to a warm reimaged focal plane is realized using reflective optics based on an aberration compensated parabolic relay [14] optimized using biconic surfaces, which ensures good optical performance over a very large field of view. The cold optics aberrations are corrected by the warm optics mounted in front of the cryostat

Manuscript received June 29, 2018; revised August 17, 2018; accepted September 10, 2018. Date of publication September 19, 2018; date of current version December 11, 2018. *(Corresponding author: Lorenza Ferrari.)*

L. Ferrari, S. J. C. Yates, and M. Eggens are with the SRON—Netherlands Institute for Space Research, 9747 AD Groningen, The Netherlands (e-mail: l.ferrari@sron.nl; S.Yates@sron.nl; m.eggens@sron.nl).

A. M. Baryshev is with the Kapteyn Institute, University of Groningen 9747, AD Groningen, The Netherlands (e-mail: a.baryshev@rug.nl).

J. J. A. Baselmans is with SRON—Netherlands Institute for Space Research, 3584 CA Utrecht, The Netherlands, and also with the TeraHertz Sensing Group, Delft University of Technology, 2628 CD Delft, The Netherlands (e-mail: J.Baselmans@sron.nl).

Color versions of one or more of the figures in this paper are available online at http://ieeexplore.ieee.org.

Digital Object Identifier 10.1109/TTHZ.2018.2871365

300 K window. The cold mirrors are enclosed in an optics box to improve stray light control and reduce loading on the pixels. The detector array pixels sample the focal plane with a sampling of approximately 1Fλ, resulting in a pixel spacing of 2 and 1 mm for the 350 and 850 GHz arrays. The power absorbed per pixel is estimated from the optical design to be 10 pW for the 350 GHz band and 40 pW for the 850 GHz design when a 77 K load is used to illuminate the detector arrays. The F# of the optical system is defined by a 3 K Lyot stop at the pupil plane, which is possible due to the directivity of the lens-antenna pixels; absorber coupled devices would need a sub-K Lyot stop [15]. At the entrance, there is a cold aperture that behaves as an effective field stop.

Additionally, the temperature of the detector array must be 250 mK or lower. At this temperature, an Aluminum MKID camera pixel (given a Tc for Al of 1.1 K) is dominated by the power received, while thermal effects are negligible [16]. The lowest base temperature is achieved by means of an He10 sorption cooler, which is a series of an He4-He3-He3 sorption cooler [17], providing 4 μW cooling power at 250 mK.

A fast turnaround of roughly a week is required to allow efficient optimization and tests of different arrays.

III. Detailed Design

The full system design is shown in Fig. 2. In the following sections, each subcomponent is described in detail including the reasoning behind our choices.

A. Reimaging Optics and Optics Box

Submm radiation is coupled through a vacuum window and reaches the detector array via reflective optics. The choice of reflective optics is driven by the high optical efficiency requirement at 850 GHz. The employment of refractive optics has been discarded for various reasons. Plastic lenses, made for example of high density polyethylene (HDPE), suffer from reflections and absorption losses. Silicon lenses have low losses but need complex antireflection coatings due to the high refractive index, which is very demanding for a wide band of 350–850 GHz. In addition, Si machining is more difficult and therefore more expensive than mirror fabricating. Another advantage of the reflective optics is that the mirrors and the 4 K optics box can be made of the same material, reducing problems related to different thermal contraction coefficients and thermal conductions at low temperature. In our case, the mirrors and optics box are made of Al 6061-T6.

The other main design drivers are: 1) near telecentric behavior, in order to have a little position dependent sensitivity or beam shape and uniform illumination over the field of view; 2) a magnification of 3 at the warm focal plane position to properly sample the pixel beam pattern; 3) good stray light control with baffles and a cold stop; and 4) the optics should be physically achievable with millimeter-scale tolerances. A constraint in the design was the presence of the magnetic shield around the sample, which limits the access angle of the array to the first mirror.

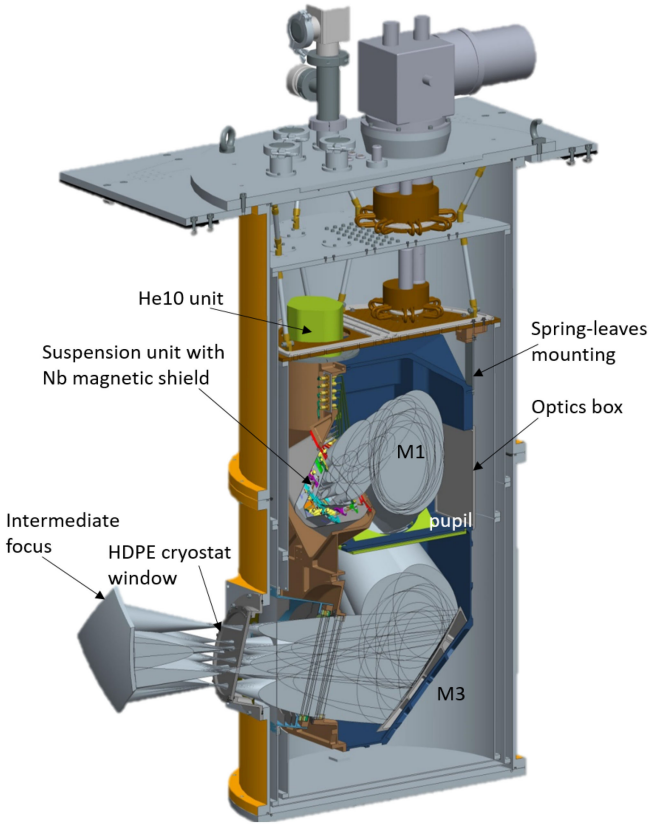

Fig. 2. Schematic of the cryostat design. From the reimaged focal plane, the radiation is entering the cryostat via am 8-mm-thick HDPE window and infrared IR scatterers. The array is mounted on a thermal–mechanical suspension unit, shown in detail in Fig. 8, which provides the mechanical interface to the optics box. The suspension unit is connected via copper thermal straps to the 850 mK ^{4}He stage, the 350 mK ^{3}He interhead stage, and the ^{3}He cold stage of the He10 cooler. The use of all these temperatures reduces the thermal load on colder stages. This entire thermal–mechanical unit and the sample holder is surrounded by a Niobium Nb superconducting magnetic shield.

Taking in account the requirements and the constraints, a starting design of two parabolic relays was chosen because it is perfect on axis and it has low aberrations dominated by field curvature off axis. The optical system was designed using Zemax [18]. All mirrors were modeled as biconics, allowing different curvature and conic constants in x and y directions. All curvatures and conic constants were set as variables, with some corrections to allow beam steering and refocus on later mirrors. The merit function was set with the main parameter, the Strehl ratio at each field point; 10 points were used with the central points having higher weights. In addition, magnification, x and y beam opening angles, and distortion were constrained. After optimization, a Strehl ratio better than 97% could be achieved over the entire field of view. The optimization introduced three flat fold mirrors to make the design physically possible and to correct for beam steering. In Fig. 3, the final design is shown. The distance between the first mirror and the array is 28 cm at an offset angle of 40°, this allows sufficient space for magnetic shield. From the array to the intermediate focus, the optics is placed in the cold at 4 K mounted inside the optics box, while the rest is external to the cryostat. A magnification of 3, in two steps of $\sqrt{3}$, is used. The modeled quality of the optics is shown

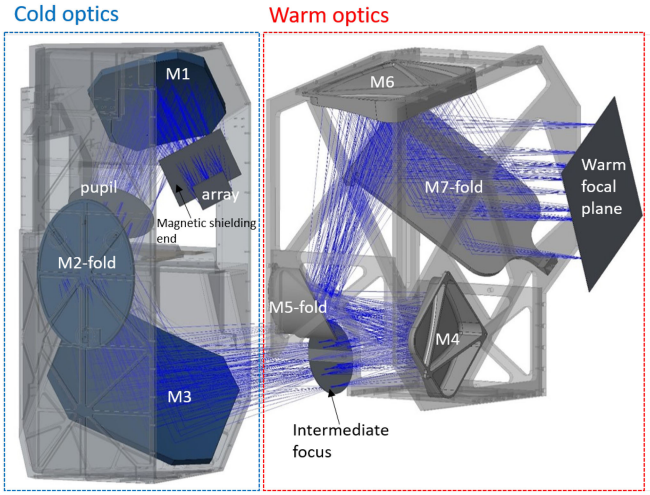

Fig. 3. Optimized optics design including fold mirrors and ray trace from field points used. The cold and warm optics is clearly distinguishable. The warm optics is mounted on a frame that is put in front of the cryostat entrance.

in Fig. 4. In addition to the geometrical calculations, a Zemax Physical optics POP study was performed for a more realistic beam shape.

The last step to perform in an optical design is the tolerances analysis, to verify the actual feasibility of the design. Two aspects were investigated: thermal and displacement tolerances. The first was studied by modeling all distance and shapes as Aluminum with a thermal contraction factor of 13×10^{-6} mm/K. The shrinking of the elements causes a drop at some field positions of the Strehl ratio to 92%. However, this could be corrected with a 12 mm defocus of the image plane, recovering a Strehl ratio higher than 97% at all field positions. The displacement tolerance study shows that the optics is relatively insensitive to displacement in the plane perpendicular to the beam (*xy* plane). *Z* plane can be corrected with refocus, resulting in a tolerance of 1° optical tilt (3 cm change in focus) and 2 mm displacement of all components or surfaces.

The cold optics is mounted inside the optics box: an enclosed box of $800 \times 425 \times 400$ mm^3 mounted on the 4 K cryostat plate via spring-leaves, which are necessary to compensate the different thermal shrinking ratio of the Copper cryostat 4 K plate and the Aluminum optics box. Each mirror has three mounting pads that allow fine positioning. The alignment of all mirrors was verified by measuring their position compared to the design with a three-dimensional measuring machine Mitutoyo Crysta-C Apex 776, each element was found to be within 0.1 mm of the designed position. The optics box also provides the mounting interface for the He10 cooler, numerous baffles coated with radiation absorber, which is a mixture of 1 mm SiC grains and Stycast 2850 [19], used to terminate radiation that does not couple to the array, and a mounting interface for the thermal–mechanical suspension unit on which the array is mounted.

As mentioned before, the box is made of Aluminum, reducing weight compared to copper. The disadvantage is the reduced thermal conductivity. This was solved by additional thermal straps, used to connect the box in different parts to the 3 K plate. The thermal straps are made in house using Copper

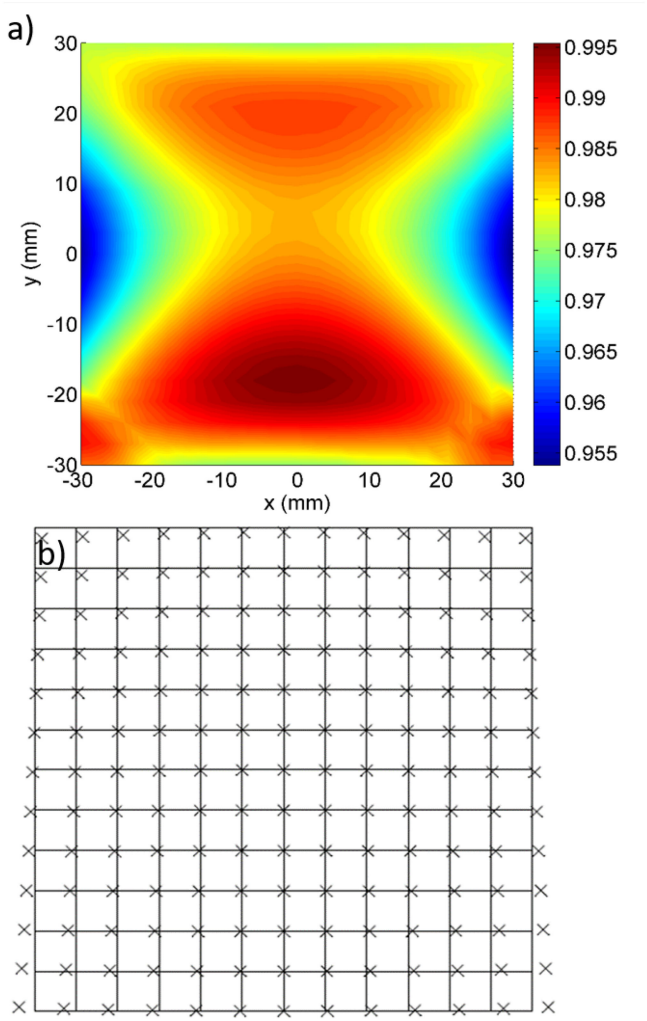

Fig. 4. (a) Variation in Strehl ratio across the focal plane. The image quality is excellent. (b) Grid distortion, position of central rays from different field points in focal (object) plane on the image plane. A small distortion of about 5% is calculated. The distortion is calculated taking the ratio of the max pixel displacement in *x* and *y* direction correcting for the hexagonal grid placement of actual pixels.

E-Cu7 (Cu > 99.9%) and they consist of braids crimped, welded, and annealed in a vacuum oven at 700° for 3 h. The usage of braids instead of a solid piece is to allow flexibility, necessary to avoid stress introduced by the thermal shrinking.

B. Radiation Filtering and Band Selection

The radiation entering the cryostat is filtered to the desired frequency band in two steps. First, we reject infrared and optical frequencies with ∼60 dB rejection in order to fully suppress the out of band contribution of the 300 K blackbody spectrum and self-emission of the windows and filters, as shown in Fig. 5. This is achieved using a combination of different types of filters mounted at 300, 50, and 4 K: thermal scatter filters, shaders, and metal mesh low-pass filters [20], [21]; the mounting order is shown in Fig. 6. A significant and known problem is the filter heating [21] due to the low thermal conduction of the substrate used for the mesh filters in combination with the big physical

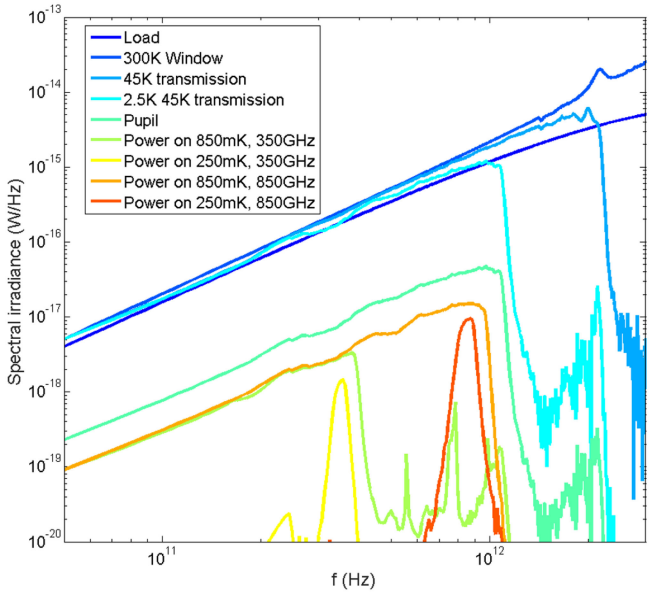

Fig. 5. Irradiance at the various temperature stages of the cryostat. The load from the laboratory environment or re-emission of hot filters is increasing with frequency and therefore high outer band rejection is crucial. Noted the above includes the reduction in throughput at each stage dominated by the cold stop.

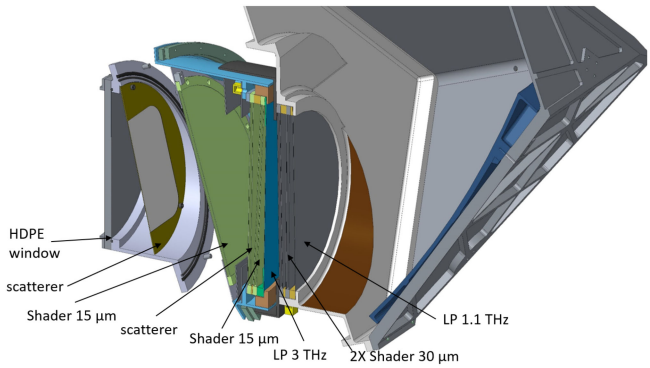

Fig. 6. Scheme of the filters mounted at 300, 50 and 4 K.

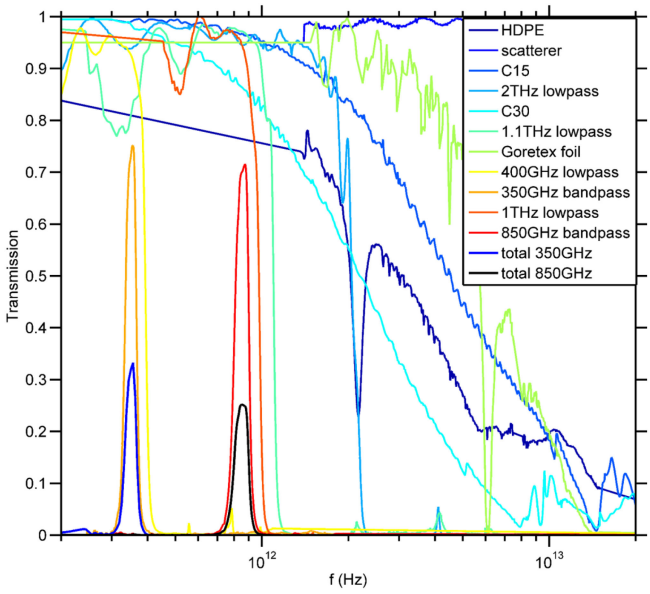

Fig. 7. Spectral transmission of the filters used in our system. C15 and C30 are two thermal shaders types: C15 is a 15-μm low-pass mounted on the 50 K temperature stage and the C30 is a 30-μm low-pass mounted on the 4 K temperature stage. Maximum transmission in band is 0.42 for the low-frequency band and 0.3 for the high-frequency band.

TABLE I
FILTER STACK PLUS RADIATIVE LOADING PER STAGE

Position	Filters	Aperture size	Power transmitted
300 K	HDPE window scatterer	∅ 168 mm	9.8 W
45 K	2X C15 shaders 2 THz low pass	∅ 200 mm	12 mW
3 K	2X C30 shaders 1.22 THz low pass	∅ 200 mm	1.8 mW
pupil	HDPE window goretex sheet	∅ 140 mm	0.1 mW
end magnetic shield (850 mK) array (250 mK)	400 GHz low pass or 1 THz low pass 350 GHz bandpass or 850 GHz bandpass	100X100 mm^2 75X75 mm^2	2.1 μW or 26 μW 0.2 μW or 2.7 μW

size (∅ 20 cm). We have confirmed the heating problem in our cryostat by measuring the temperature of the 4 K 1.1-THz low-pass filter at the entrance of the optics box to be 32 K. This is low enough to block the re-emitted power with the remaining filters. Each of them serves a specific goal. The HDPE absorbs infrared radiation and remits at all angles. The scatterer scatter near infrared and optical radiation and reduce condensation on the HDPE entrance window. The thermal shaders reflect mid and far infrared power back out of the cryostat. The low passes reflect out of band millimeter radiation below 2 THz, and above 2 THz they become grey and absorb. The Goretex sheet is mounted together with an HDPE window on the pupil stop inside the optics box within an angle and it absorbs and scatters around unwanted radiation that will be absorbed by the coating of the box.

The second part of the filtering depends on the frequency band we want to use: at the entrance of the magnetic shield of the thermal–mechanical structure, we mount a metal-mesh low-pass filter; on the detector array, we mount a band defining metal mesh filter [20]. The details of the filters are given in Table I: a first-order approximation of the power loading is the power transmitted, a more realistic calculation includes the estimate of the emissivity, thermal conductivity, and effect of multiple reflections.

The measured transmission of all filters is shown in Fig. 7. This is used to calculate the expected optical loading on the array for two sets of loads: we consider a liquid nitrogen load filling, the beam in front of the cryostat and a 300 K load. The second is the maximum power falling on the KID array setting a requirement on the cooling power at the cold stage (see Table I). The sky loading at the telescope is predicted to be between these two values. The 300 K case is taken as thermal design driver for our testbed.

C. Cooling Unit

The cooling system consists of a commercial two-stage pulse tube cooler (PTC) with 50 W cooling power at 50 K and 1 W

TABLE II
OPERATING TEMPERATURES AND COOLING POWERS OF THE CRYOSTAT STAGES

Stage	T[K]	P_{cool}
50 K (PT)	45	50 W
4 K (PT)	3	0.5 W
^{4}He buffer head	850 mK	200 μW
intermediate head ^{3}He	350 mK	50 μW
ultra cold head ^{3}He	250 mK	4 μW

TABLE III
THERMAL LOADING FROM THE KID READOUT COMPONENTS

Stage	Type	Mechanical loading
50 K (PT)	10 CuNi coax	0.25 W
4 K (PT)	10 CuNi coax	20 mW
4 K (PT)	5 LNA amplifiers	25 mW
850 mK stage	10 CuNi coax	40 μW
350 mK	10 CuNi coax	1 μW

cooling power at 4 K, which is mounted inside the cryostat itself. This is a commercial system from Entropy cryogenics [22]. We added an in-house liquid nitrogen precooling system (LN2) and the He10 sorption cooler. The LN2 precooling system is made of stainless steel tubes with a diameter of $\varnothing$ 6 mm and a wall thickness of 1 mm, combined with commercial vacuum connector components with special thermally isolated feedthroughs and a copper exchanger mounted on the 4 K plate. The LN2 flows via the tubes and cools down the cryostat plates to roughly 80 K, two times faster than the PT cooler alone, allowing for a fast turnaround of the system. The stainless steel of the tubes has a low thermal conductivity, therefore the cryostat stages are practically thermally isolated when the precooling is not in use.

The He10 sorption cooler is a three-stage, two single shot systems consisting of ^{3}He cold heads and an ^{4}He buffer head. The buffer head is used to condense the ^{4}He (850 mK) and to cool down the intermediate cold head (350 mK), which acts as a buffering for the ultracold stage. In this way, the heat load on the ultracold head is reduced and hence the operating temperature lowered (250 mK) and the operating time increased. The He10 provides by design a factor of two in margin in the cooling power and it is easy to operate.

We summarize in Table II the thermal properties of the cryostat stages, indicating the operating temperature of each level and the cooling power available.

D. Readout

The KID readout system consists of coaxial cables and amplifiers to connect the external readout system [23] to the detector array for a total of five readout chains. The readout signal is fed into the cryostat by standard coaxial cables with SMA connectors with double dc blocks at the input of the cryostat to prevent ground loops. The signal runs from 300 K to the detector array and back. At 4 K, a -20 dB attenuator is added and at 0.85 K, a -10 dB signal attenuator is added to reduce the 300 K thermal noise to values corresponding to below 1 K. In the suspension unit, the signal before reaching the detectors passes through a single dc block. After the array, the signal is transferred back via a single dc block to the 4 K stage where it gets amplified by a dual stage Yebes 4–8 GHz low noise amplifier LNA [24] with 5 K noise temperature and 1 dB compression point at -31 dBm input power. Inside the cryostat, we use from 300 to 4 K 2.19 mm diameter coax cables made of CuNi with an Ag cladding on the central conductor [25], a choice dictated by the low thermal conductivity and high flexibility. From 4 K to the outer side of the optics box, we use 0.86 mm diameter copper coax cables, since both are at the same temperature and close to each other. To bring the signal from the inner side of the box to the detector array and viceversa, we use 0.86 mm diameter CuNi coax cables with an Ag cladding on the central conductor. We prefer to use CuNi coax instead of NbTi for their robustness. We can allow for the extra loss, which increases the noise contribution from our LNA, because the noise contribution of the multiplexed readout is higher than the LNA contribution when reading out $\sim$1000 MKIDs [13]. All the cables have an extra length and are bent in place for stress relief and thermalization. In Table III, the thermal loading calculated from the system readout at each temperature level is summarized. From the 350 mK to the 250 mK stage, the thermal loading is negligible. The loading expected in all stages is by design more than a factor 2 lower than the cooling power available from the PTC and He10, as shown in Table III compared to Table II.

In addition to the microwave readout, the cryostat has dc readout harness made of Phosphorbronze. The dc harness is used for the readout of thermometers, operating the He10 and the power supply of the LNA. The wires for the heaters and low noise amplifiers are 0.2 mm thick, due to the higher current sent through, instead of the 0.1 mm thickness used for the thermometers. The wires are thermally anchored with clamping structures to the temperature levels of the cryostat and the heat load is negligible (a factor of 100) compared to the loading from the coax cables (see Table III).

E. Suspension Unit

The detector array is thermally isolated and cooled down to 250 mK using a thermal suspension unit in a volume of 170 $\times$ 170 $\times$ 110 mm^3 (see Fig. 8). The unit is mounted at the outside of the optics box, providing a mechanical interface at 3 K. The thermal suspension contains two additional intermediate temperature levels at 850 and 350 mK to reduce the thermal load to the 250 mK detector unit. The temperature levels are provided by the He10 cooler via flexible thermal straps, the same type used for the optics box and described before. All temperature stages consist of square annular decks, which are separated using three supports in a isostatic configuration. The supports are made of Vespel SP1, because of the low thermal conductivity ($1.8 * 10^{-3}$ W/m*K @1K), high specific strength (60 kN*m/kg @RT), and good manufacturability properties. Between two decks, the same supports are used where each triangular shaped support has two legs with a cross section of 1.2 mm $\times$ 2.6 mm over a length of 10 mm each. The thermal contraction point is chosen to be the central optical axis in order to minimize misalignment of the detector unit during cooling down and differences in thermal expansion of the used materials. All decks

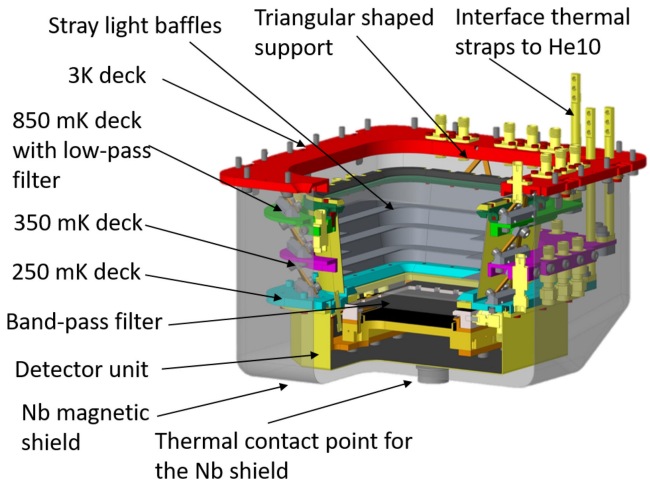

Fig. 8. Schematic of the thermal suspension unit: each subcomponent is indicated.

TABLE IV
SUSPENSION UNIT POWER LOADING

Stage	Type	Loading	Total
850 mK	10 CuNi coax	40 μW	
850 mK	3 Vespel supports	18 μW	
850 mK	optical	2.1μW (350 GHz)	60 μW (350 GHz)
850 mK	optical	26 μW (850 GHz)	84 μW (850 GHz)
350 mK	10 CuNi coax	1 μW	1.5 μW
350 mK	3 Vespel supports	0.5 μW	
250 mK	optical	0.2 μW (350 GHz)	0.2 μW (350 GHz)
250 mK	optical	2.7 μW (850 GHz)	2.7 μW (850 GHz)

are made of copper C11000 except the deck, which is interfacing to the optics box. This deck is made of the same material as the optics box, Aluminum 6061-T6, to avoid stress due to differences in thermal expansion at cryogenic temperatures.

The deck at 850 mK is equipped with a low-pass filter for the last low-pass filter and a baffle. The inner side of the baffle is coated with the same absorbing material as the box. The signal harness is thermally coupled to each deck to reduce the thermal load at the detector unit and the necessary cable length is achieved by rerouting and crossing over. In Table IV, the thermo–mechanical loading at the different stages of the suspension unit are summarized. The attenuators, dc-blocks, and connectors are used to rigidly clamp the coaxial harness to the decks.

The detector array is mounted using springs and clamps in a light tight sample holder with a bandpass filter mounted on front. To attenuate magnetic fields, the whole thermal suspension is surrounded with a niobium superconducting shield with a thickness of 0.5 mm. The shield has a cup shape and an aspect ratio of 0.44 providing 100 times reduction of stray magnetic field at the detector location. The magnetic shield is thermally isolated from the optics box and has a separate central thermal contact point to cool down the shield separately from its apex to press out flux upon cooling. This is to avoid freezing in permanent magnetic fields.

To avoid stray light, we introduce meander structures with absorbing coating for the mounting interface of the magnetic shield and of the light tight environment of the detector unit.

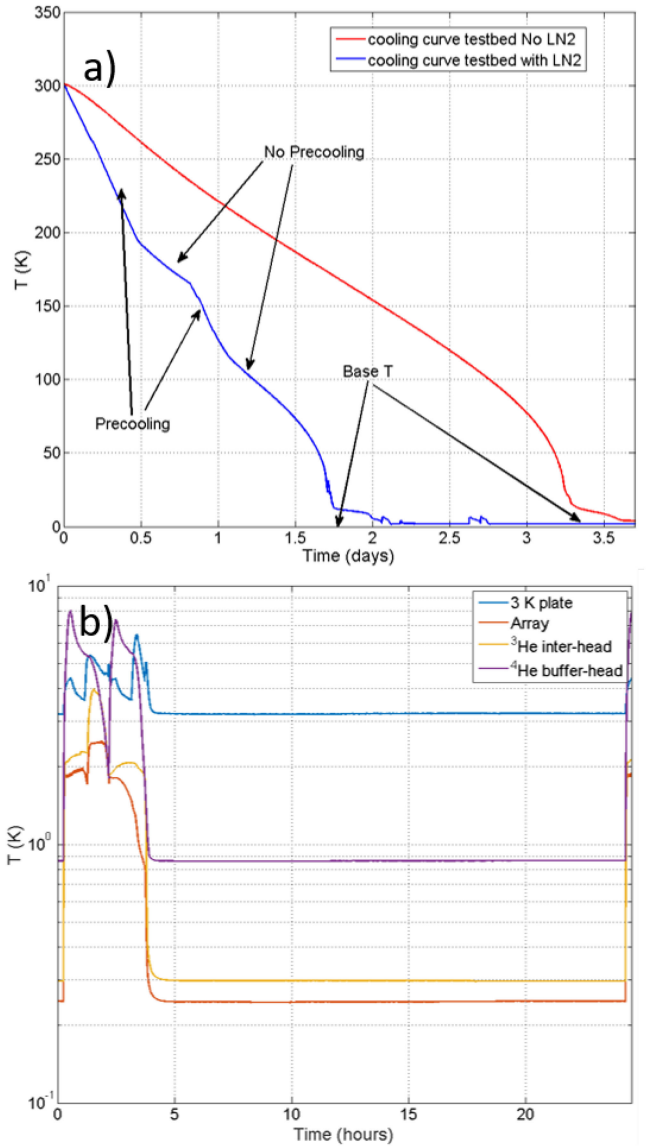

Fig. 9. (a) Cooling curves of our testbed with and without using the LN2 precooling. In case of use of the precooling, the cryostat reaches base temperature in roughly two days instead of four. In the precooling curve, we have indicated with the arrows "No precooling" the moments when the liquid nitrogen run out and the cooling of the system slowed down. (b) Zoom in of the He10 cooldown and the array.

The detector holder can be exchanged easily by dismounting the magnetic shield and detector unit cover.

IV. PERFORMANCE VERIFICATION

The thermal operation of the cryostat shows excellent performance (see Fig. 9) confirming the validity of our thermo–mechanical modeling. The 250 mK base temperature is reached in roughly two days despite the big physical dimension and masses of the testbed. The hold time at the lowest temperature is about 30 h with an additional recharge of the ^{4}He buffer head with a temperature stability of about 5 mK.

The verification of the camera performance includes the measurements of the detector sensitivity and how well the radiation

is coupled to the array. The sensitivity is defined as noise equivalent temperature (NET), which quantifies how sensitive the camera is in measuring temperature variation. The NET measurement consists of determining the signal to noise on a calibration load that fills the entire field of view. In our case, the load is given by a blackened SiC sheet immersed in liquid nitrogen, resulting in a temperature of 90 K assuming 93% emissivity of the sheet. The procedure for the NET measurement is the following: the first step consists in finding the focus position of the reimaged focal plane by scanning a wire grid in different *Z* planes parallel to the optics exit aperture (*XY* is in the focal plane); the focus corresponds to the minimum in the beam size. Once we are in focus, a wire grid scan determines the pixel position. Then, the first parameter to measure for the calculation of the NET is the KID responsivity: namely the variation in frequency response (and thus kinetic inductance) related to a variation in temperature of the optical signal, which is linearly proportional to the power in the Rayleigh–Jeans limit. The responsivity is measured by means of a knife edge scan [26], a Goretex strip is scanned in the reimaged focal plane on top of the laboratory load. The strip is slightly gray in band adding a signal of 21 K on top of the 90 K of the load, the strip has been previously calibrated with a polarizer grid and LN2 load. The other quantity to measure is the noise, which is instrument related as this sets the photon background. The noise is determined from a time stream on the load of about 1 min taking at 100 Hz to remove 1/f of the nitrogen load. A separate noise measurement of a stable load showed a 1/f knee to be below 0.5 Hz, probably corresponding to the two-level system TLS noise level [27]. The system noise is estimated from the KID amplitude noise level [27] and dominated by the readout contribution [13] which is ∼10 dB below the detector photon noise.[1] The detector photon noise is evaluated from the noise by subtracting the system contribution. In Fig. 10, a typical NET map for a 350 GHz array is shown. The map demonstrates background limited operation for the detectors over the entire focal plane in agreement to within 10% of the theoretical NET expected from the cryostat. This has been validated using calibrated detectors [9], [10], previously tested in other facility and fully characterized.

Finally, the verification of the optics quality is realized by the comparison between the measured beam patterns and the simulated POP beam patterns from Zemax for both detector bands. The agreement is excellent for the 350 GHz data, see Fig. 11; in the 850 GHz beam, the measured data are undersampled anyway and the agreement is very good. The beam patterns are measured with the phase and amplitude technique described in detail in [28].

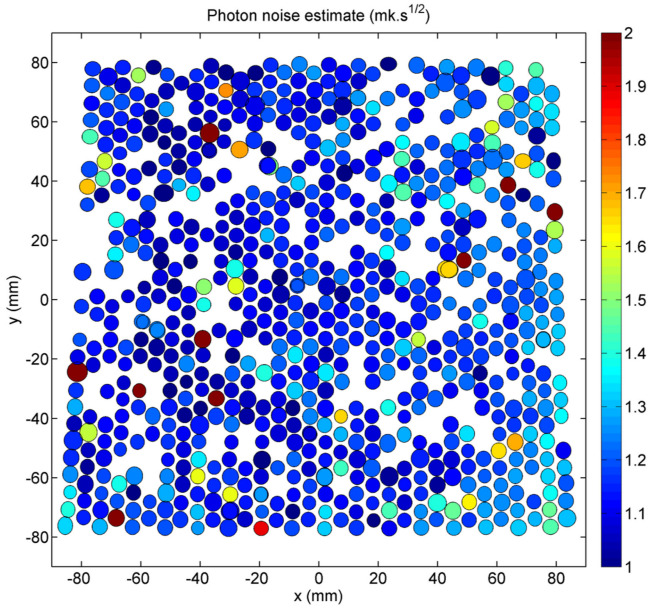

Fig. 10. Map of photon noise NET in mK*s$^{0.5}$ showing background limited operation over the entire focal plane. The array tested is a 880 pixels 350 GHz array. The NET is quite uniform over the entire array and the beams have a circular shape in good agreement with the optical model. The orientation of the NET map corresponds to the orientation of the grid distortion map showed in Fig. 4(b). The measured distortion is equal to 8.5%, in good agreement with the 5% calculated from the Zemax model, confirming the good quality of our optics model.

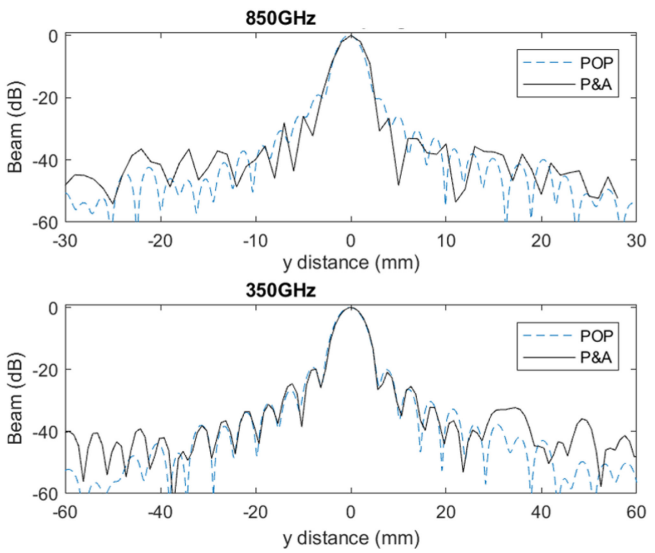

Fig. 11. Comparison between beam patterns measured using phase and amplitude technique and the Zemax POP simulations for a 350 and 850 GHz detector. The agreement is excellent, and in the case of the 850 GHz array the beam pattern measured is slightly undersampled.

V. Conclusion

We have described the process for successfully designing and building a wide field camera measuring large format KID arrays and have verified that it meets the required performance. The cryostat reaches a base temperature of 250 mK in roughly two days and it has an hold time of about 30 h with an additional recharge of the He10 buffer head. The thermo–mechanical modeling is in agreement with the measured performance. The quality of the optics has also been verified by the comparison of the measured and simulated beam patterns and excellent

[1]Due to the number of bits in the ADC at 1000 tones, we have a noise level of around −98 dBc/Hz. At −70 dBm readout power, this corresponds to around 250 K noise temperature. However, with our detectors, the readout noise is still 10 dB below the detector photon noise.

agreement is obtained. The 350 GHz detectors show photon noise limited background operation, confirming the quality of the radiation coupling system.

ACKNOWLEDGMENT

The authors would like to thank R. van der Schuur and J. Panman for their help and support during the assembly and operations of the cryostat. The authors would also like to thank G. Keizer for his help, in particular for the design and fabrication of the thermal straps.

REFERENCES

[1] P. K. Day, H. G. Leduc, B. A. Mazin, A. Vayonokis, and J. Zmuidzinas, "A broadband superconducting detector suitable for large array," *Nature*, vol. 425, pp. 817–821, 2003.
[2] W. S. Holland *et al.*, "SCUBA-2: The 10000 pixel bolometer camera on the James Clerk Maxwell Telescope," *Monthly Notices Roy. Astronom. Soc.*, vol. 430, no. 4, pp. 2513–2533, 2013.
[3] V. Reveret *et al.*, "The ArTÉMiS wide-field submillimeter camera: Preliminary on-sky performances at 350 microns," *Proc. SPIE*, vol. 9153, Jun. 2014, Art. no 915305. [Online]. Available: http://dx.doi.org/10.1117/12.2055985
[4] J. Sclaerth *et al.*, "A millimeter and sumillimeter kinetic inductance detector camera," *J. Low Temp. Phys.*, vol. 151, no. 3-4, pp. 684–689, 2008.
[5] A. Monfardini *et al.*, "NIKA: A millimeter-wave kinetic inductance camera," *Astron. Astrophys.*, vol. 521, 2010, Art. no. A29.
[6] R. Adam *et al.*, "Substructure and merger detection in resolved NIKA Sunyaev-Zel'dovich images of distant clusters," *Astron. Astrophys.*, vol. 614, 2018, Art. no. A118. [Online]. Available: https://doi.org/10.1051/0004-6361/201731950
[7] 2015. [Online]. Available: http://hss.ulb.uni-bonn.de/2015/4094/4094.htm
[8] APEX telescope. 2003. [Online]. Available:www.apex-telescope.org
[9] L. Ferrari *et al.*, "Antenna coupled MKID performance verification at 850 GHz for large format astrophysics arrays," *IEEE Trans. Terahertz Sci. Technol.*, vol. 8, no. 1, pp. 127–139, Jan. 2018.
[10] R. M. J. Janssen *et al.*, "High optical efficiency and photon noise limited sensitivity of microwave kinetic inductance detectors using phase readout," *Appl. Phys. Lett.*, vol. 103, 2013, Art. no. 203503.
[11] CCAT telescope. 2012. [Online]. Available: www.ccatobservatory.org
[12] At-LAST telescope. [Online]. Available: http://www.eso.org/sci/publications/announcements/sciann17050.html
[13] J. van Rantwijk, M. Grim, and D. Van Loon, "Multiplexed readout for 1000-pixel arrays of microwave kinetic inductance detectors," *IEEE Trans. Microw. Theory Techn.*, vol. 64, no. 6, pp. 1876–1883, Jun. 2016. [Online]. Available: http://dx.doi.org/10.1109/TMTT.2016.2544303
[14] J. A. Murphy, "Distortion of a simple gaussian beam on reflection from off-axis ellipsoidal mirrors," *Int. J. Infrared Milli. Waves*, vol. 8, no. 9, pp. 1165–1187, Sep. 1987. [Online]. Available: http://dx.doi.org/10.1007/BF01010819
[15] M. Calvo *et al.*, "The NIKA2 instrument, a dual-band Kilopixel KID array for millimetric astronomy," *J. Low Temp. Phys.*, vol. 184, pp. 816–823, 2016.
[16] P. J. de Visser *et al.*, "Number fluctuations of sparse quasiparticles in a superconductor," *Phys. Rev. Lett.*, vol. 106, 2011, Art. no. 167004.
[17] Chase Research Cryogenics Ltd. 1993. [Online]. Available: http://www.chasecryogenics.com/
[18] Zemax LLC, "Zemax optical studio," 2013. [Online]. Available: http://www.zemax.com
[19] J. A. Baselmans, S. J. C. Yates, P. Diener, and P. J. de Visser, "Ultra low background cryogenic test facility for far-infrared radiation detectors," *J. Low Temp. Phys.*, vol. 167, pp. 360–366, 2012.
[20] QMC Instruments Ltd, 2008. [Online]. Available: http://www.terahertz.co.uk/qmc-instruments-ltd
[21] C. E. Tucker and P. A. R. Ade, "Thermal filtering for large aperture cryogenic detector arrays," *Proc. SPIE*, vol. 6275, 2006, Art. no. 62750T.
[22] Entropy Cryogenics. 2011. [Online]. Available: http://www.entropy-cryogenics.com/
[23] J. J. A. Baselmans *et al.*, "A kilo-pixel imaging system for future space based far-infrared observatories using microwave kinetic inductance detectors," *Astron. Astrophys.*, vol. 601, May 2017, Art. no. A89.
[24] I. Lopez-Fernndez, C. Diez, J. D. Gallego, and A. Barcia, "Wide band cryogenic IF amplifiers for ALMA and herschel receivers," in *Proc. 14th Int. Symp. Space Terahertz Technol.*, Apr. 2003, pp. 502–504.
[25] COAX CO. LTD. 1974. [Online]. Available: http://www.coax.co.jp/en/
[26] L. Bisigello, S. J. C. Yates, V. Murugesan, J. J. A. Baselmans, and A. M. Baryshev, "Calibration scheme for large kinetic inductance detector arrays based on readout frequency response," *J. Low Temp. Phys.*, vol. 184, no. 1, pp. 161–166, 2016. [Online]. Available: http://dx.doi.org/10.1007/s10909-016-1524-x
[27] J. Gao *et al.*, "A semiempirical model for two-level system noise in superconducting microresonators," *Appl. Phys. Lett.*, vol. 92, 2008, Art. no. 212504.
[28] K. K. Davis *et al.*, "Proof-of-concept demonstration of vector beam pattern measurements of kinetic inductance detectors," *IEEE Trans. THz Sci. Technol.*, vol. 7, no. 1, pp. 98–106, Jan. 2017. [Online]. Available: http://dx.doi.org/10.1109/TTHZ.2016.2617869

Lorenza Ferrari received the Ph.D. degree in applied physics (working on cryogenic detectors for astrophysics applications) from the University of Genoa, Genoa, Italy, in 2009.

After that, she was with the INFN Genoa and PTB Berlin, Germany, for one year, as a Postdoctoral Researcher involved with low temperature detectors for neutrino mass experiments. Since 2010, she has been an Instrument Scientist with SRON—Netherlands Institute for Space Research, Utrecht, The Netherlands. Her current interests include the development of microwave kinetic inductance detectors for sub-mm applications and transition edge sensors for FAR-IR frequency range, focussing on optical characterization and application in scientific instruments. She is also involved in the SpicA FAR-Infrared Instrument and X-Ray Integral Field Unit Spectrometer experiments modeling and testing the focal plane assembly, as well as designing cryogenic facilities for performance validation of instruments components.

Stephen J. C. Yates received the Ph.D. degree (working on experimental low temperature techniques for condensed matter physics) from the University of Bristol, Bristol, U.K., in 2003.

He then was with the CNRS-CRTBT (now Institut NÉEL), Grenoble, France, as a Postdoctoral Researcher involved with low temperature magnetism and superconductivity (2003–2004). He followed this also at CNRS-CRTBT with work on the development of low temperature detectors and techniques for astrophysics (2004–2006). He is currently an Instrument Scientist working on superconducting microwave kinetic inductance detectors (MKIDs) at SRON—Netherlands Institute for Space Research, Utrecht, The Netherlands, which he started in 2006. His current interests include MKID development for sub-mm applications, and also a wider interest in device physics and superconductivity, optical design, and full end-to-end instrument characterization and performance.

Martin Eggens received the B.Sc. degrees in mechanical engineering and electrical engineering from Hogeschool Drenthe, Emmen, The Netherlands, in 1995 and 1997, respectively.

Since then, he has been a Mechanical Design Engineer with SRON—Netherlands Institute for Space Research, Groningen, The Netherlands. He is mainly involved in engineering of optomechanical design, analysis (vibration, thermal), alignment, and mechanisms of cryogenic space instrumentation and ground equipment.

Andrey M. Baryshev received the M.S. degree (*summa cum laude*) in physical quantum electronics from the Moscow Physical Technical institute, Moscow, Russia, in 1993, and the Ph.D. degree in superconducting integrated receiver combining SIS mixer and flux flow oscillator into one chip from the Technical University of Delft, Delft, The Netherlands, in 2005.

He is currently an Associate Professor with the Kapteyn Astronomical Institute, University of Groningen, Groningen, The Netherlands. He was previously a Senior Instrument Scientist with SRON—Low Energy Astrophysics Division, Groningen, The Netherlands, from 1998 to 2017. In 1993, he was an Instrument Scientist with the Institute of Radio Engineering and Electronics, Moscow, Russia, involved in the field of sensitive superconducting heterodyne detectors. In 2000, he joined an effort to develop an SIS receiver (600–720 GHz) for the Atacama Large Millimeter Array, where he designed the SIS mixer, quasi-optical system, and contributed to a system design. His current main research interests include application heterodyne and direct detectors for large focal plane arrays in terahertz frequencies and quasi-optical systems design and experimental verification.

Dr. Baryshev was the recipient of the NOW-VENI Grant for his research on heterodyne focal plan arrays technology in 2008 and, in 2009, he was the recipient of the EU commission Starting Researcher Grant for his research on focal plane arrays of direct detectors.

Jochem J. A. Baselmans received the graduation degree and Ph.D. degree (*summa cum laude*) from the University of Groningen, Groningen, The Netherlands, in 1998 and 2002, respectively. His disseration was entitled "Controllable Josephson Junctions."

He is a Senior Instrument Scientist with SRON—Netherlands Institute, Groningen, where, since 2002, where he has been with the Technology Division. Since 2015, he has also been an Associate professor with the Terahertz Sensing Group, Delft University of Technology, Delft, The Netherlands. He started in 2002 as Postdoctoral Instrument Scientist with SRON—Netherlands Institute for Space Research, where, until 2004, he was involved with hot electron bolometer mixers, very sensitive heterodyne radiation detectors for frequencies between 1 and 5 THz. In 2005, he joined SRON Utrecht, and began working on microwave kinetic inductance detectors (MKIDs) after a three month visit to the California Institute of Technology, Pasadena, CA, USA. In 2015, he received an ERC Consolidator Grant to develop an advanced imaging spectrometer based upon MKIDs. He now leads the Dutch effort on the development of MKIDs. He has authored or co-authored publications in excess of 100 papers.